JOM
https://doi.org/10.1007/s11837-020-04522-9
© 2021 The Minerals, Metals & Materials Society

ADVANCED COATING AND THIN FILM MATERIALS FOR ENERGY, AEROSPACE AND BIOLOGICAL APPLICATIONS

Peculiarities of Intermetallic Phase Formation in the Process of a Solid State Reaction in $(Al/Cu)_n$ Multilayer Thin Films

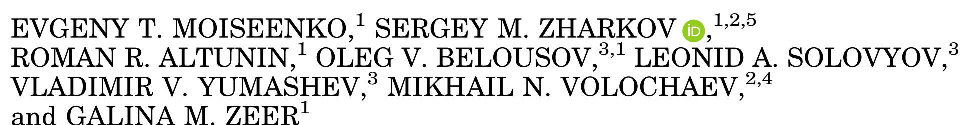

EVGENY T. MOISEENKO,[1] SERGEY M. ZHARKOV,[1,2,5] ROMAN R. ALTUNIN,[1] OLEG V. BELOUSOV,[3,1] LEONID A. SOLOVYOV,[3] VLADIMIR V. YUMASHEV,[3] MIKHAIL N. VOLOCHAEV,[2,4] and GALINA M. ZEER[1]

1.—Siberian Federal University, 79 Svobodny pr., Krasnoyarsk, Russia 660041. 2.—Kirensky Institute of Physics, Federal Research Center KSC SB RAS, Akademgorodok 50/38, Krasnoyarsk, Russia 660036. 3.—Institute of Chemistry and Chemical Technology, Federal Research Center KSC SB RAS, Akademgorodok 50/24, Krasnoyarsk, Russia 660036. 4.—Reshetnev Siberian State University of Science and Technology, Krasnoyarskij Rabochij 31, Krasnoyarsk, Russia 660037. 5.—e-mail: zharkov@iph.krasn.ru

Phase formation in a solid state reaction in Al/Cu bilayer and multilayer thin films was studied by the methods of in situ transmission electron microscopy, electron diffraction, simultaneous thermal analysis and x-ray diffraction. It was established that the phase formation sequences in the $(Al/Cu)_n$ (n = 2, 15) multilayer thin films (θ-Al_2Cu $\rightarrow$ γ_1-Al_4Cu_9 $\rightarrow$ η_2-AlCu) and Al/Cu bilayer thin films (θ-Al_2Cu $\rightarrow$ η_2-AlCu $\rightarrow$ γ_1-Al_4Cu_9) were different. It was assumed that the phase formation process in the thin films was strongly affected by a number of copper/aluminum interfaces due to the changes of aluminum and copper diffusion current.

INTRODUCTION

Copper and aluminum are widely used in microelectronics and power engineering. Multilayer films containing aluminum are promising for nanojoining[1,2] applied as reactive nanofoils.[3,4] Aluminum-copper alloys are being considered for their further use as metal coatings[5] and absorbers[6] in complementary metal-oxide semiconductor technology. The techniques of joining aluminum and copper are being widely studied, in particular, friction welding[7–9] and thermosonic wire bonding.[10,11] Copper cladding aluminum is a material which has potential for energy transmission.[12–14] Here, special attention is paid to the formation processes of intermetallic compounds at the aluminum-copper interface, and, in particular, to the phase formation sequence as the formation of intermetallic compounds. This is important since the formation of intermetallic compounds can result in a considerable change in the physical properties of the materials. So, for example, in Ref. 15, it is shown that the formation of intermetallic compounds Al_2Cu and Al_4Cu_9 on the interface of Cu/Al during the thermosonic Cu-wire bonding process results in increasing strength of the copper aluminum compound. In Ref. 16, it is established that the Al_4Cu_9 phase makes the largest contribution to the mechanical strength of the copper-aluminum compound, while the Al_2Cu phase is extremely fragile and brittle at room temperature. As far as the electrical properties are concerned, in Refs. 8 and 17, it is shown that the formation of intermetallic compounds on the interface of Cu/Al results in an increase of the electrical resistivity. In Ref. 18, it is shown that the Al-Cu phase is subjected to corrosion while the Cu_9Al_4 and $CuAl_2$ phases are corrosion-resistant.

According to the diagram of phase equilibria[19] in the Al-Cu system, the formation of the following intermetallic compounds is possible: θ-Al_2Cu; η_2-AlCu, η_1-AlCu; ξ_2-Al_3Cu_4, ξ_1-Al_3Cu_4; δ-Al_2Cu_3, ε_2-Al_2Cu_3, ε_2-Al_2Cu_3; γ_1-Al_4Cu_9, γ_0-Al_4Cu_9; α_2-$AlCu_3$, β-$AlCu_3$, and β_0-$AlCu_3$. As predicted by the effective heat of formation model (EHF),[20–22] intermetallic compounds are formed at the aluminum-copper interface according to the following sequence: θ-Al_2Cu $\rightarrow$ η_2-AlCu $\rightarrow$ ξ_2-Al_3Cu_4 $\rightarrow$ δ-Al_2Cu_3 $\rightarrow$ γ_1-Al_4Cu_9 $\rightarrow$ α_2-$AlCu_3$. The fact that the θ-Al_2Cu

(Received September 5, 2020; accepted December 2, 2020)

Published online: 04 January 2021

phase is the first to be formed has been experimentally confirmed in a number of studies.[10,17,22–28] However, as far as any further sequence of the phase formation is concerned, the researchers present rather different data. The studies can be subdivided into several groups based on the phase sequences observed: Al + Cu → θ-Al_2Cu → γ_1-Al_4Cu_9;[23,24] Al + Cu → θ-Al_2Cu → η_2-AlCu → γ_1-Al_4Cu_9;[25,26] and Al + Cu → θ-Al_2Cu → γ_1-Al_4Cu_9 → η_2-AlCu.[10,17,27,28] However, one should note that most of these results have been obtained by ex situ methods which have prevented the authors from establishing the exact formation sequence for the intermetallic phases at the aluminum-copper interface.

This study presents the results of a complex investigation of the process of the solid-state reaction in Al/Cu bilayer and multilayer films by the methods of in situ transmission electron microscopy (TEM), electron diffraction (ED), x-ray powder diffraction (XRD), simultaneous thermal analysis (STA), including differential scanning calorimetry (DSC), and thermogravimetry (TG). The character of the reaction process in thin films is known to be considerably different depending on the number and thickness of the reacting layers.[29] The application of in situ TEM and ED methods allows one to record new phases appearing in the process of the solid-state reaction at the initial stages of the reaction product formation.

EXPERIMENTAL PROCEDURES

The investigated Al/Cu bilayer and $(Al/Cu)_n$ multilayer thin films were obtained by magnetron sputtering on an EPOS-PVD-D-CONFOCAL high-vacuum setup. The base pressure was better than 1×10^{-4} Pa and the argon pressure during magnetron sputtering was 0.26 Pa. The number of bilayers (n) in the multilayer films was equal to 2 and 15. The individual layer thickness in the bilayer and multilayer thin films was 30 ± 1 nm for the Al layer, and 50 ± 1 nm for the Cu layer. The material deposition rate was Al at 0.4 nm/s and Cu at 0.8 nm/s. The layer thickness and deposition rate were controlled using a Bal-Tec QSG-100 quartz crystal thickness monitor. The twoinch (c. 50-mm) targets (Girmet) with a purity—Cu (99.997%) and Al (99.999%) were mounted on Onyx 2-inch magnetrons (Angstrom Sciences). The substrates used for the film deposition were glass and electron microscopy grids (Ted Pella) made from nickel and coated with a thin (~ 20 nm) amorphous carbon layer.

The microstructure and the local elemental composition of the samples were studied using a JEM-2100 (JEOL) TEM equipped with an Oxford Inca x-sight energy dispersive spectrometer (EDS) at an accelerating voltage of 200 kV. The elemental compositions of the multilayer films were studied using a JSM-7001F (JEOL) SEM equipped with an Oxford Inca Energy 350 at an accelerating voltage of 15 kV.

To conduct the in situ investigation of the solid-state reaction process, films deposited on an amorphous carbon layer located on TEM grids (Ted Pella) were used. The solid-state reaction was initiated by the thermal heating of the samples directly in the column of the TEM with the help of a heating sample holder (Gatan Model 652 Double Tilt Heating Holder). The authors successfully used the method to investigate the process of the solid-state reaction in thin film bilayer nanosystems: Al/Cu,[22] Al/Ag,[30] Al/Pt,[31] Al/Fe,[32] Cu/Au,[33] Fe/Pd,[34,35] Fe/Si,[36] Zr/Fe_2O_3,[37] Zr/Co_3O_4,[38] In/Co_3O_4,[39] etc.

Also, to conduct the TEM investigations and to study the solid-state reaction process, cross-section samples of the multilayer thin films were prepared by a focused ion beam using a Hitachi FB-2100 (40 kV accelerating voltage) with subsequent Ar^+ polishing at 0.5 kV.

The XRD data were collected at 25°C on a PANalytical X'Pert PRO diffractometer operating with CuK_a radiation (1.541874 Å) in the scan range from 5° to 110° 2θ (step width = 0.02° 2θ; time per step 10 s). Phase identification was performed by making reference to the ICDD PDF 4 + Release 2020 database.[40]

The simultaneous thermal analysis of an Al-Cu sample (the sample was molded at a pressure of 53.1 MPa for 3 min) was performed on a Jupiter STA 449C analyzer (Netzsch) with a Aëolos QMS 403C quadrupole mass spectrometer (Netzsch) in Pt-Rh crucibles with perforated lids, using a sample portion of 18 mg. The measurement of the mass change (TG, DTG), the heat flux (DSC), and the composition of gaseous products (by Ar^+, O_2^+, CO_2^+, CO^+, H_2O^+, and SO_2^+ molecular ions) were performed in the regime of linear increase in the temperature at a rate of 10°C/min within the temperature range of 50–400°C, cooling to 50°C and further heating to 400°C in a dynamic gas atmosphere supplying 99.999% Ar gas (total flow rate, 50 cm^3 STP/min). The sensitivity of the DSC/TG sensor was determined using the heat capacity of a standard sapphire disc; the relative ΔH detection error did not exceed 4%. The heat effect values refer to the initial portion.

RESULTS AND DISCUSSION

The TEM investigation (Fig. 1a) of the $(Al/Cu)_2$ films in the initial state demonstrates that the films are composed of crystallites having the size of 15 ± 5 nm. The analysis of the selected area electron diffraction (SAED) pattern obtained from the area with the diameter of 1.3 μm (Fig. 1b) shows the presence of polycrystalline reflections corresponding to face central cubic (FCC) phases of copper (PDF card #00-004-0836, space group Fm-3 m, lattice constant a = 3.615 Å) and aluminum (PDF card #00-004-0787, space group Fm-3 m, lattice constant a = 4.049 Å). Study of the elemental composition using the method of EDS shows the aluminum

content in the $(Al/Cu)_2$ films to be 25.4 ± 0.5 at.%, with the copper content being—74.6 ± 0.5 at.% (Fig. 1c). On the EDS spectrum, low-intensity peaks related to Ni, Fe and Co are also observed, but their appearance is explained by the peculiarities of conducting EDS in TEM. The signal from Ni is due to the Ni TEM grid, while the Fe and Co signals are from the TEM pole-piece.

For the purpose of studying the phase formation processes in the solid-state reaction in the $(Al/Cu)_2$ system, the films were heated to 300°C at a heating rate of 4°C/min. During the heating, SAED patterns were recorded. As a result, a set of the SAED patterns was obtained and processing these data allowed the building of the temperature dependence of the phase volume content in the solid-state reaction process in the $(Al/Cu)_2$ system (Fig. 2). The technique of processing the electron diffraction patterns is described in detail in Ref. 22.

The analysis of the temperature dependences of the phase volume content in the solid-state reaction process (see Fig. 2) shows that the reaction began at ≈ 87°C, which corresponds to the reaction initiation temperature in the bilayer Al/Cu films.[22] The first phase to form during the reaction was θ-Al_2Cu (PDF card #00-025-0012, space group I4/mcm, lattice constants: $a = b = 6.065$ Å, $c = 4.873$ Å). At the beginning of the reaction, the first changes appeared in the SAED patterns: low intensity diffraction reflections corresponding to the interplanar distances $d(110) = 4.29$ Å and $d(200) = 3.03$ Å of the θ-Al_2Cu phase. The fact that the θ-Al_2Cu phase was the first to form corresponds both to the theoretical predictions of the EHF model[20–22] and to the results obtained in experimental studies.[10,22–28]

The second phase to form at 122°C was γ_1-Al_4Cu_9 (PDF card #01-074-7041, space group P43-m, lattice constant $a = 8.685$ Å). The SAED patterns reveal the appearance of diffraction reflections having a low intensity and corresponding to $d(210) = 3.89$ Å of the γ_1-Al_4Cu_9 phase.

At 143°C, the phase η_2-AlCu began to form in the film (PDF card #00-026-0016, space group C2/m, lattice constants: $a = 12.066$ Å, $b = 4.105$ Å, $c = 6.913$ Å). However, the maximum content of the η_2-AlCu, phase formed in the sample did not exceed ≈ 1 vol.% (see Fig. 2).

The analysis of the SAED pattern obtained from the $(Al/Cu)_2$ sample after heating to 300°C (Fig. 3) shows that, in the film, along with the γ_1-Al_4Cu_9 phase, there exists the α_2-$AlCu_3$ phase,[41,42] an ordered solid solution of Cu(Al) with the lattice constant $a \approx 3.67$ Å. The lattice constant of the solid solution is ≈ 1.5% higher than the lattice parameter of copper ($a = 3.615$ Å), which corresponds to the solid solution with the composition of $Al_{19}Cu_{81}$.[19] It is necessary to note that, in the analysis of the dependence of the phase volume composition (see Fig. 2), there was no possibility to separate the phase content of pure copper and that of the Cu(Al) solid solution formed in the solid-state reaction process. However, it was found that, after heating to 300°C, no pure copper was observed in the film, only the $Al_{19}Cu_{81}$ solid solution and the γ_1-Al_4Cu_9 being present.

Earlier, in some studies,[24,28] it was shown that, at a rather high ratio of Cu:Al as a result of a solid-state reaction, a mixture of the phases γ_1-Al_4Cu_9 and Cu was formed. According to the phase diagram of the system Al-Cu,[19] the mixture of the phases γ_1-Al_4Cu_9 and α_2-$AlCu_3$ (PDF card #01-080-4572, space group Pm-3 m, lattice constant: $a = 3.69$ Å) exists in the concentration range of 68.0–76.5 at.% Cu at a temperature lower than 363°C. The latter, in its turn, is a solid solution of Cu(Al) ordered according to the Cu_3Au type with the lattice constant $a = 3.69$ Å.[41,42] One should note that the main reflections of the α_2-$AlCu_3$ phase almost coincide with the reflections of FCC copper and Cu(Al) disordered solid solution. The superstructure reflections of α_2-$AlCu_3$ $d_{011} = 2.60$ Å are close to the reflections of Al_4Cu_9 $d_{311} = 2.62$ Å, which does not allow their use to identify the presence of the α_2-$AlCu_3$ phase. However, in the electron diffraction pattern obtained after heating to 300°C (see Fig. 3), one can observe the reflections $d \approx 3.67$ Å, corresponding to the interplanar distances $d_{001} = 3.69$ Å of the α_2-$AlCu_3$ phase. Thus, it is possible to state that, as a result of the solid-state reaction in the $(Al/Cu)_2$ thin films with the atomic ratio of Al:Cu ≈ 25:75 at.%, a mixture of the γ_1-Al_4Cu_9 and α_2-$AlCu_3$ phases is formed. However, it is not possible to determine the starting temperature for the formation of the Cu(Al) disordered solid solution in the solid-state reaction in the $(Al/Cu)_2$ multilayer thin films due to the fact that all the reflections almost coincide with those of the FCC copper phase. It is also impossible to determine the starting temperature of the α_2-$AlCu_3$ phase—Cu(Al) ordered solid solution, because the main characteristic reflection ($d_{001} = 3.69$ Å) allowing the identification of the phase has a rather low intensity (∼ 10%).

Based on the experimental results of the present research, it becomes possible to establish the following formation sequence of the phases in the solid-state reaction in the $(Al/Cu)_2$ thin film nanosystem (the atomic ratio being Al:Cu ≈ 25:75):

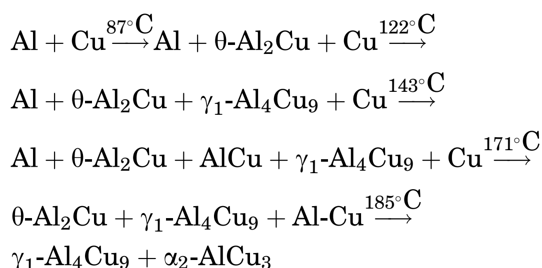

$$\mathrm{Al + Cu} \xrightarrow{87^\circ\mathrm{C}} \mathrm{Al} + \theta\text{-}\mathrm{Al_2Cu} + \mathrm{Cu} \xrightarrow{122^\circ\mathrm{C}}$$
$$\mathrm{Al} + \theta\text{-}\mathrm{Al_2Cu} + \gamma_1\text{-}\mathrm{Al_4Cu_9} + \mathrm{Cu} \xrightarrow{143^\circ\mathrm{C}}$$
$$\mathrm{Al} + \theta\text{-}\mathrm{Al_2Cu} + \mathrm{AlCu} + \gamma_1\text{-}\mathrm{Al_4Cu_9} + \mathrm{Cu} \xrightarrow{171^\circ\mathrm{C}}$$
$$\theta\text{-}\mathrm{Al_2Cu} + \gamma_1\text{-}\mathrm{Al_4Cu_9} + \mathrm{Al\text{-}Cu} \xrightarrow{185^\circ\mathrm{C}}$$
$$\gamma_1\text{-}\mathrm{Al_4Cu_9} + \alpha_2\text{-}\mathrm{AlCu_3}$$

It is necessary to note that the γ_1-Al_4Cu_9 phase was formed earlier than the η_2-AlCu phase, which contradicts the predictions of the EHF model. The sequence (Al + Cu → θ-Al_2Cu → γ_1-Al_4Cu_9 → η_2-AlCu) observed in the present study differs from the phase formation sequence obtained earlier by the

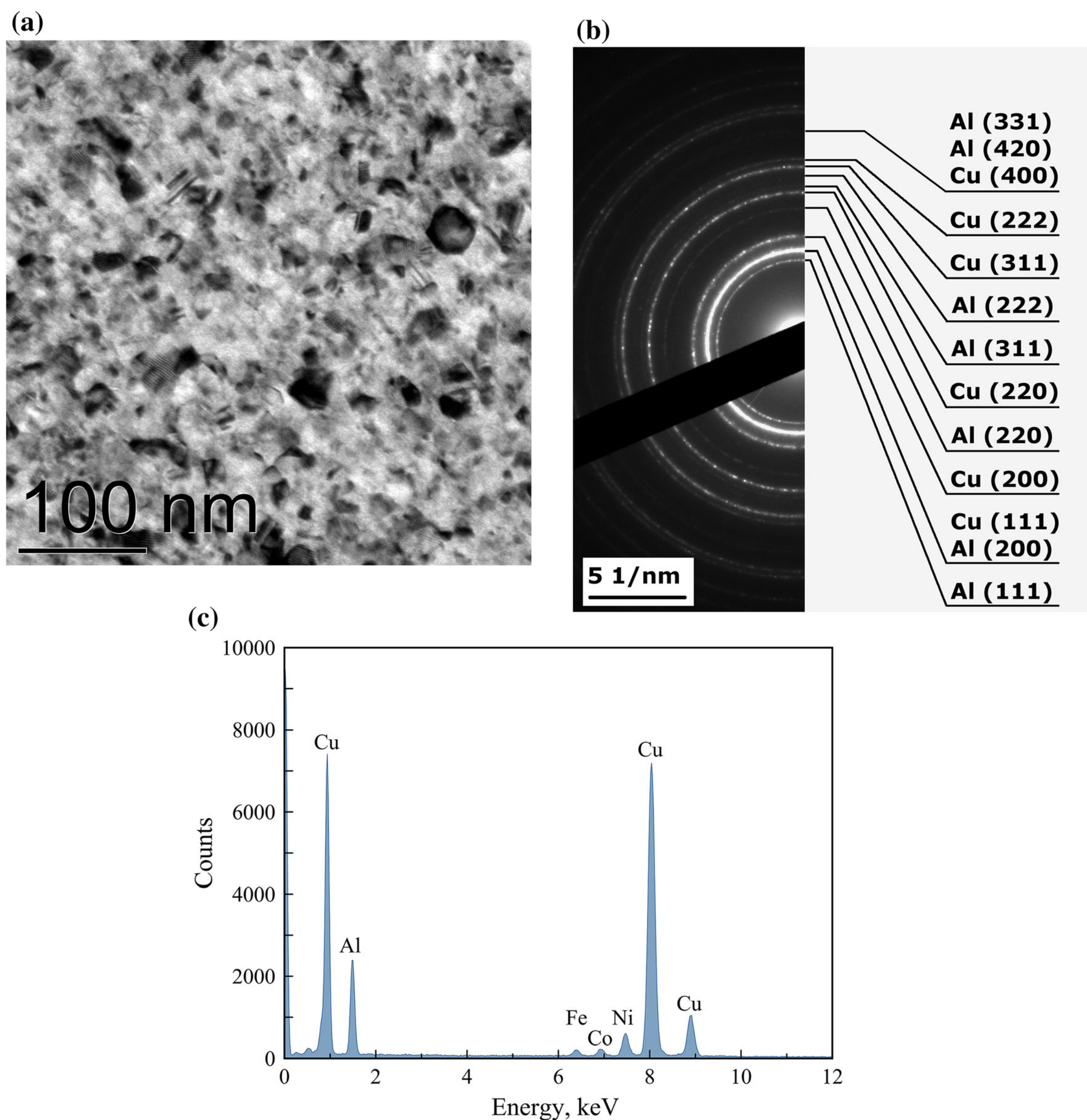

Fig. 1. Bright-field TEM image (a), SAED pattern (b), and EDS spectrum (c) obtained from the $(Al/Cu)_2$ film at the initial state.

authors in the solid-state reaction in Al/Cu bilayer thin films with the atomic ratio Al:Cu = 31:69 (Al + Cu → θ-Al_2Cu → η_2-AlCu → γ_1-Al_4Cu_9),[22] in which the starting formation temperature for the γ_1-Al_4Cu_9 phase in the $(Al/Cu)_2$ films (122°C) is much lower than that in the Al/Cu bilayer films.

The present study also involves the study of the formation processes of intermetallic phases in the solid-state reaction in the Al/Cu bilayer thin films with the atomic ratio Al:Cu ≈ 25:75, which results in establishing that the phase sequence (θ-Al_2Cu → η_2-AlCu → γ_1-Al_4Cu_9) and the starting temperature of the phase formation for Al_4Cu_9 (195°C) are similar to those obtained earlier in Ref. 22. It is worth noting that the thickness of the individual aluminum and copper layers both in the Al/Cu bilayer films and in the $(Al/Cu)_n$ multilayer films (n = 2, 15), were identical: the thickness of aluminum is ≈ 30 nm while that of the copper layer is ≈ 50 nm.

Thus, it is possible to assume that, at comparable thicknesses and atomic ratios of aluminum and copper, the sequence and initiation temperatures of the formation of the intermetallic compounds θ-Al_2Cu, η_2-AlCu, and γ_1-Al_4Cu_9 in the solid-state reaction at the interface of the aluminum and copper depends only on the number of bilayers, i.e., on the number of interfaces of Al/Cu.

To test the abovementioned assumption, a study of the solid-state reaction processes was carried out in the process of heating $(Al/Cu)_{15}$ thin multilayer films. The thicknesses of the individual aluminum

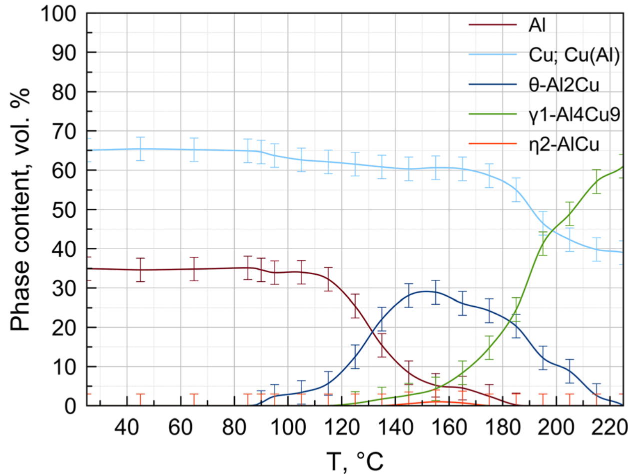

Fig. 2. Dependence of the volumetric content of the phases Al, Cu, θ-Al_2Cu, γ_1-Al_4Cu_9, and η_2-AlCu on the temperature in the process of heating the $(Al/Cu)_2$ film.

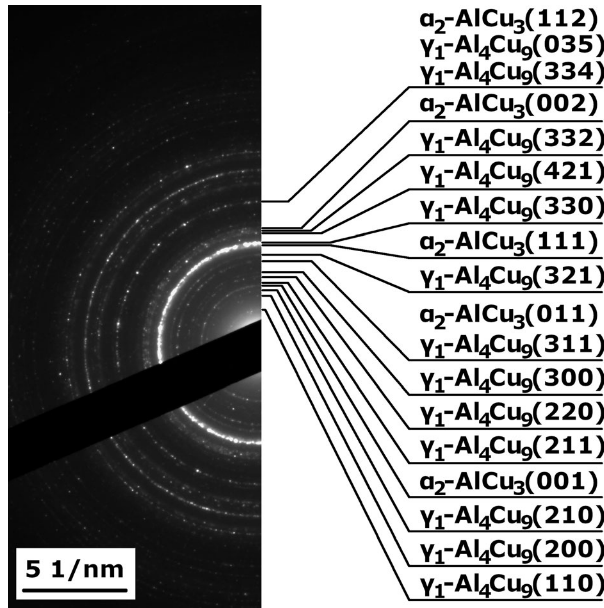

Fig. 3. SAED pattern obtained from the $(Al/Cu)_2$ film at 300°C.

layers were 30 ± 1 nm, and those of the copper 50 ± 1 nm. The elemental content of aluminum and copper in the $(Al/Cu)_{15}$ films was equal to Al of 25.3 ± 0.5 at.%, and Cu of 74.7 ± 0.5 at.%. This was determined by the EDS method (see Fig. 4) conducted in SEM from the film located on a glass substrate, and the area of the analysis was 100 μm^2. Thus, the thicknesses of the individual layers and the aluminum-copper ratio were identical to those in the Al/Cu and $(Al/Cu)_2$ films. Figure 5a and b presents a TEM image of a cross-section and the XRD pattern of a $(Al/Cu)_{15}$ multilayer film in the initial state. The observed reflections (see Fig. 5b) correspond to the FCC phases of aluminum and copper. The analysis of the intensity of the

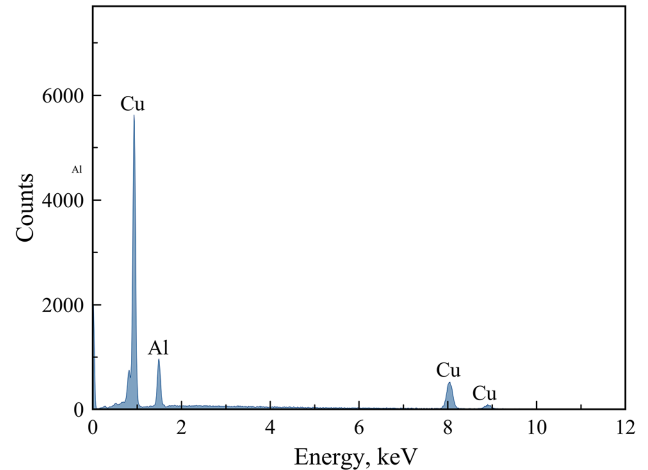

Fig. 4. EDS spectrum obtained in SEM from the $(Al/Cu)_{15}$ multilayer film after annealing at 350°C.

diffraction reflections indicates that there exists in the film the predominant orientation of the aluminum and copper crystallites, the atomic planes of the Cu(111) type and Al(111) type being parallel to the substrate plane.

The study of the phase formation processes in the solid-state reaction by the methods of in situ bright-field TEM and ED was carried out in the "cross-section" geometry in the process of thermal annealing in the column of the TEM: 100°C for 25 min, 150°C for 45 min, 250°C for 25 min, and 350°C for 25 min. The first changes in the TEM images obtained from the $(Al/Cu)_{15}$ films were recorded in the process of annealing at 150°C. At the interfaces of the aluminum and copper layers during the first minutes of annealing at 150°C, one could already observe the appearance of single crystallites of a new phase (Fig. 6a). In this case, the crystallites of the new phase were formed in the aluminum layer at the interface of the aluminum and copper. This is due to the fact that the diffusion coefficient of copper into aluminum is higher than that of aluminum diffusion into copper (the diffusion coefficients of aluminum and copper were calculated based on the data presented in Ref. 17, and were equal to $D_{Cu \to Al} = 1.33 \times 10^{-17}$ cm^2/s at 150°C; $D_{Cu \to Al} = 1.72 \times 10^{-21}$ cm^2/s). The analysis of the ED patterns shows that these were the crystallites of the θ-Al_2Cu phase (Fig. 6b). Further, during the annealing at 150°C, increases in the number and size of the crystallites of the θ-Al_2Cu phase were observed. Thus, the analysis of the bright-field TEM images and SAED patterns obtained from the cross-section of $(Al/Cu)_{15}$ in the process of thermal annealing confirms that the θ-Al_2Cu phase is the first to form in the solid-state reaction in the $(Al/Cu)_{15}$ thin films. During the annealing at 250°C and 350°C, the subsequent growth of the crystallites of × Al-Cu intermetallic compounds was observed.

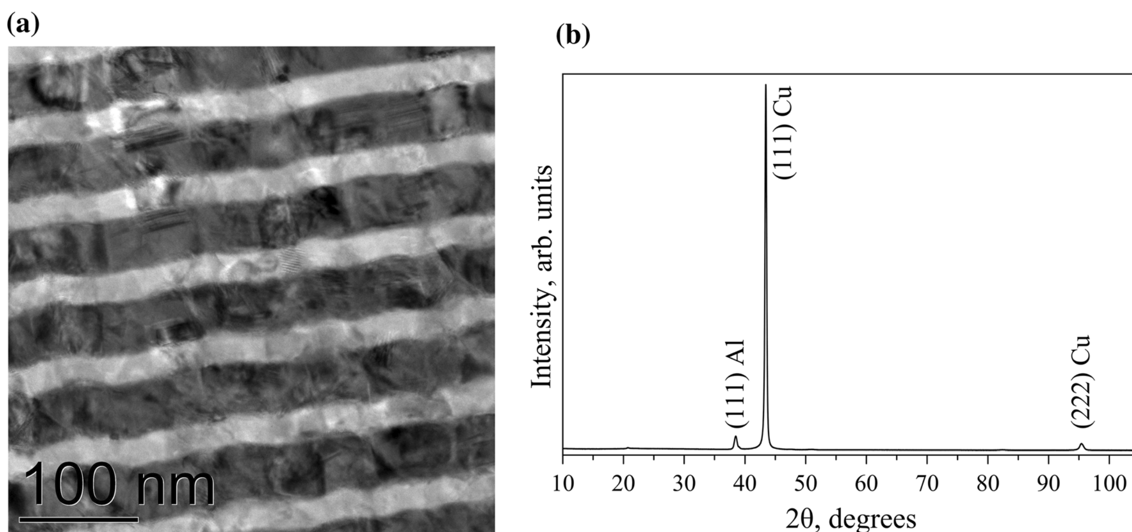

Fig. 5. Cross-section TEM image (a) and XRD pattern of a $(Al/Cu)_{15}$ multilayer film at the initial state (b), obtained from the $(Al/Cu)_{15}$ multilayer film at the initial state.

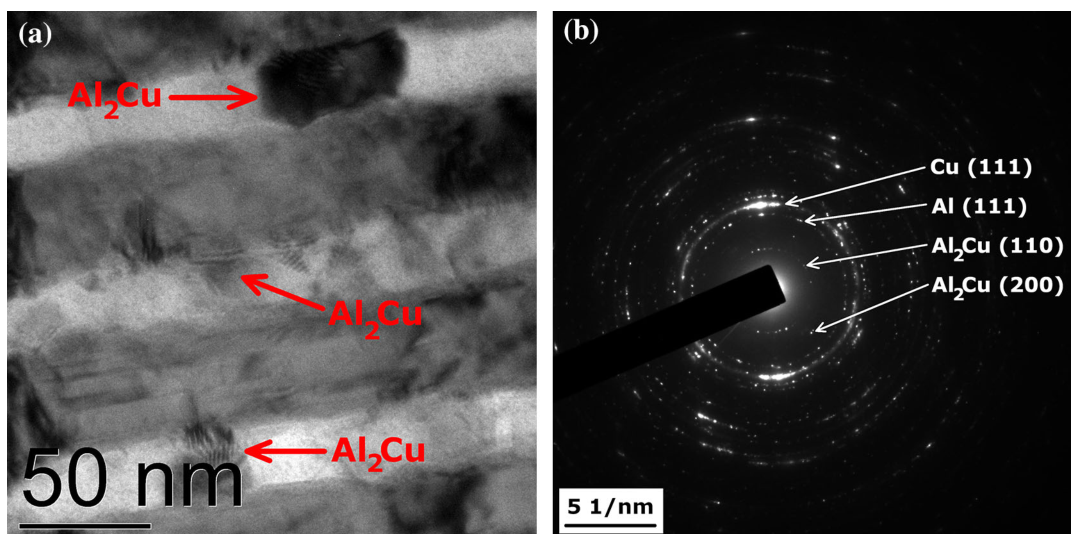

Fig. 6. Cross-section TEM image (a) and SAED pattern obtained from the $(Al/Cu)_{15}$ multilayer film at 150°C (b).

The analysis of the SAED (Fig. 7a) and XRD patterns (Fig. 7b) obtained from the samples after annealing shows that, as a result of the solid-state reaction in the $(Al/Cu)_{15}$ multilayer films, similar to the $(Al/Cu)_2$ films, a mixture of the phases γ_1-Al_4Cu_9 and α_2-$AlCu_3$, i.e., Cu(Al) solid solution was formed. In the case of the XRD pattern (see Fig. 7b), one can see two high-intensity reflections: 2θ = 44.063°, corresponding to γ_1-Al_4Cu_9 d(330) = 2.055 Å, and 2θ = 42.697°, corresponding to $d(111)$ = 2.118 Å of the Cu(Al) solid solution with the lattice constant = 3.668 Å, corresponding to $Al_{19}Cu_{81}$.[19] The analysis of the XRD reflection intensity (see Fig. 7b) shows that there is the predominant crystallite orientation: the planes (330) of the phase γ_1-Al_4Cu_9 and (111) of the $Al_{19}Cu_{81}$ are parallel to the plane of the substrate. The crystallite orientation does not allow one to determine whether or not the Cu(Al) solid solution is ordered (α_2-$AlCu_3$ phase).

Simultaneous thermal analysis was carried out for the purpose of obtaining information concerning the thermophysical characteristics of the solid-state reaction processes in the $(Al/Cu)_{15}$ multilayer films. The STA analysis (see Fig. 8) shows that, in the temperature range of 90–260°C on the DSC curve (first heating), one can observe the vivid exothermic effect (ΔH = – 243 J/g), which is seen as a complex peak with the local and main maxima at 158°C and at 192°C, respectively. Moreover, on this curve,

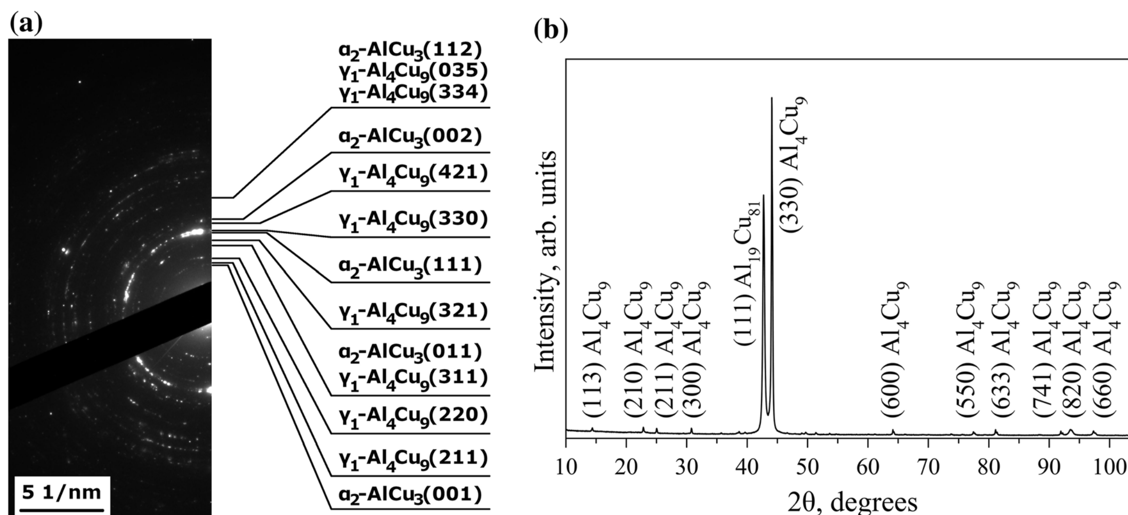

Fig. 7. Electron diffraction pattern (a) and XRD pattern (b) obtained from the (Al/Cu)$_{15}$ multilayer film after annealing at 350°C.

there exists a hidden peak in the form of a "shoulder" at 217°C (the location is specified by the second derivative of the DSC curve).

The TG curve (first heating) reveals a small drop in the sample mass in the temperature range 75–200°C, of about 0.10 wt.%, which is due to the loss of the surface OH groups (or adsorbed H_2O, m/z = 18), while at temperatures higher than 200°C an increase in mass is observed, of about 0.013 wt.%, accompanied by the formation of CO_2 (m/z = 44), probably, due to the oxidation of surface carbides (or other organic compounds) by the trace oxygen in the Ar atmosphere.

The subsequent cooling and second heating of the sample show (see Fig. 8) that the thermochemical transformation of the Al-Cu system in the temperature range under study was completed, and that any thermal effects due to the phase transformations are absent.

The complex character of the exo-thermal peak on the DSC curve (Fig. 8, DSC heating 1) allows one to assume the presence of, at least, three components (at 158, 192, and 217°C), which can be referred to different stages of the solid-state process occurring in the Al-Cu thin film system. The first peak with the maximum at 158°C can correspond to the formation of the θ-Al_2Cu phase (see Fig. 2). Here, the initiation temperatures of the solid-state reaction in the multilayer films of $(Al/Cu)_{15}$ and $(Al/Cu)_2$ according to the DSC and ED data are in good agreement: 90°C and 87°C, respectively. The formation process of the γ_1-Al_4Cu_9 phase (see Fig. 2) can be ascribed to the second peak with the maximum at 192°C (see Fig. 8, DSC heating 1). Here, the starting temperature for the formation of the given phase (130°C), according to the results of the DSC curve, is also in agreement with the starting temperature for the formation of the given phase (122°C), obtained using the analysis of the

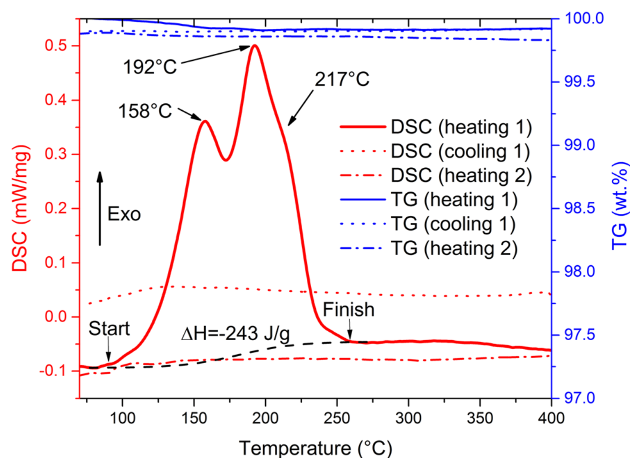

Fig. 8. DSC and TG curves obtained from (Al/Cu)$_{15}$ at heating–cooling–heating cycle (at linear temperature rate 10°C/min).

temperature dependence of the volume content in the solid-state reaction process (see Fig. 2). The third peak with the maximum at 217°C (see Fig. 8, DSC heating 1), is likely to correspond to the formation process of the Cu(Al) ordered solid solution (α_2-$AlCu_3$ phase). It is worth noting that the DSC curve does not show any vivid peak corresponding to the formation of the η_2-AlCu phase, which is explained by the fact that the given phase is formed in very small amounts ≈ 1 vol.% (see Fig. 2).

Thus, as a result of the analysis of the experimental data obtained in the present study, it is established that, at comparable thicknesses of the aluminum and copper nanolayers, and at the identical atomic ratio of aluminum and copper, the sequences of the phase formation in the solid-state reaction initiated thermal heating at a rate of 4–10°C/min, in the case of the Al/Cu bilayer films

(Al + Cu $\rightarrow$ θ-Al_2Cu $\rightarrow$ η_2-AlCu $\rightarrow$ γ_1-Al_4Cu_9) and $(Al/Cu)_n$ multilayer films (Al + Cu $\rightarrow$ θ-Al_2Cu $\rightarrow$ γ_1-Al_4Cu_9 $\rightarrow$ η_2-AlCu) are different. In particular, the phase γ_1-Al_4Cu_9 in the case of the multilayered films is formed earlier than the η_2-AlCu phase at a considerably lower temperature, as compared to the Al/Cu bilayer films. In this case, the formation of the γ_1-Al_4Cu_9 phase occurring earlier than the η_2-AlCu phase contradicts the predictions of the EHF model.

There are several possible mechanisms to suppress the formation of intermediate phases in thin films:[43]

1. "Fast is the first" model. According to the given model, the first phase to form is the one having the highest growth rate, and the phases growing slower in the presence of the fast growing phase grow even more slowly than they could.
2. Diffusion suppression of nucleation. Since in the diffusion process the nuclei of phase 2 exist in a strongly non-uniform system and participate in diffusion interactions, they can decrease to the critical sizes due to diffusion suppression by the neighboring fast growing phase 1, and, as a result, phase 2 is not formed.
3. Influence of the interface barriers. In the case when one phase is being formed, the interface barriers only decrease the phase formation rate which results in linear growth instead of parabolic. In the case of two phases, the interface barriers can make the growth rate of an individual phase formally negative, which implies that this phase will be completely absent.
4. Along with the kinetic methods, there is also a possibility of thermodynamic suppression of intermediate phase formation. Upon the formation of a phase with a narrow homogeneity range, its sharp chemical potential gradient prevents the nucleation of the subsequent phase. As a result, the thermodynamic suppression of the formation of a new phase, in addition to the kinetic one, can be efficient until the thickness of the suppressing phase remains smaller than several tens or even hundreds of nanometers.

In Refs. 23 and 44, it is established that the phases θ-Al_2Cu and γ_1-Al_4Cu_9 "are easy to nucleate and grow"; however, the η_2-AlCu phase grows slowly.[27] Thus, the most likely explanation of the changes in the phase formation sequence in the solid-state reaction in the Al/Cu bilayer and $(Al/Cu)_n$ multilayer thin films observed in this study is in the fact that, in the case of the multilayered films, the mechanism of the process changes due to the increasing diffusion current of copper resulting from a bigger number of aluminum/copper interfaces.

CONCLUSION

It has been established that the solid-state reaction initiated by thermal heating in Al/Cu bilayer and multilayer thin films starts with the formation of the θ-Al_2Cu phase presented as individual crystallites at the Al/Cu interface, both in the bilayer and multilayer thin films. However, further sequences of the phase formation were different. In the case of the Al/Cu bilayer thin films, the following phase sequence was observed: θ-Al_2Cu $\rightarrow$ η_2-AlCu $\rightarrow$ γ_1-Al_4Cu_9, which is in the agreement with the prediction of the EHF model. In the case of the multilayer thin films, the phase sequence was different: θ-Al_2Cu $\rightarrow$ γ_1-Al_4Cu_9 $\rightarrow$ η_2-AlCu. It has been assumed that the differences in the phase formation sequences were caused by suppressing the formation of the η_2-AlCu phase due to a higher diffusion current of copper provided by a larger number of Al/Cu interfaces in the case of the multilayer system. Thus, it has been shown that the phase formation process in the thin films was strongly affected by the number of interfaces.

ACKNOWLEDGEMENTS

This work was supported by the Russian Science Foundation under Grant #18-13-00080. The electron microscopy investigations were conducted in the SFU Joint Scientific Center whose infrastructure was supported by the State assignment (#FSRZ-2020-0011) of the Ministry of Science and Higher Education of the Russian Federation. The preparation of cross-section samples for TEM investigations was conducted in the Krasnoyarsk Regional Center of Research Equipment of Federal Research Center "Krasnoyarsk Science Center SB RAS".

CONFLICT OF INTEREST

The authors declare that they have no conflict of interest.

REFERENCES

1. Y.N. Zhou, eds., *Microjoining and Nanojoining* (Cambridge: Woodhead, 2008).
2. D.J. Fisher, *Bonding by Self-propagating Reaction* (Millersville: Materials Research Forum LLC, 2019).
3. A.S. Rogachev, S.G. Vadchenko, F. Baras, O. Politano, S. Rouvimov, N.V. Sachkova, M.D. Grapes, T.P. Weihs, and A.S. Mukasyan, *Combust. Flame* 166, 158 (2016). https://doi.org/10.1016/j.combustflame.2016.01.014.
4. A.S. Mukasyan, A.S. Rogachev, and S.T. Aruna, *Adv. Powder Technol.* 26, 954 (2015). https://doi.org/10.1016/j.apt.2015.03.013.
5. A.I. Oliva, J.E. Corona, and V. Sosa, *Mater. Charact.* 61, 696 (2010). https://doi.org/10.1016/j.matchar.2010.03.016.
6. M.R.S. Dias, C. Gong, Z.A. Benson, and M.S. Leite, *Adv. Opt. Mater.* 6, 1700830 (2018). https://doi.org/10.1002/adom.201700830.
7. Q.-z. Zhang, W.-b. Gong, and W. Liu, *Trans. Nonferrous Met. Soc. China* 25, 1779 (2015). https://doi.org/10.1016/S1003-6326(15)63783-9.

8. W.-B. Lee, K.-S. Bang, and S.-B. Jung, *J. Alloys Compd.* 390, 212 (2005). https://doi.org/10.1016/j.jallcom.2004.07.057.
9. A. Zykova, A. Chumaevskii, A. Gusarova, T. Kalashnikova, S. Fortuna, N. Savchenko, E. Kolubaev, and S. Tarasov, *Metals* 10, 818 (2020). https://doi.org/10.3390/met10060818.
10. H. Xu, I. Qin, H. Clauberg, B. Chylak, and V.L. Acoff, *Scr. Mater.* 115, 1 (2016). https://doi.org/10.1016/j.scriptamat.2015.12.025.
11. H. Xu, C. Liu, V.V. Silberschmidt, S.S. Pramana, T.J. White, and Z. Chen, *Scr. Mater.* 61, 165 (2009). https://doi.org/10.1016/j.scriptamat.2009.03.034.
12. D. Chu, J.-Y. Zhang, J.-J. Yao, Y.-Q. Han, and C.-J. Wu, *Trans. Nonferr. Metal. Soc. China* 27, 2521 (2017). https://doi.org/10.1016/S1003-6326(17)60279-6.
13. T.T. Sasaki, R.A. Morris, G.B. Thompson, Y. Syarif, and D. Fox, *Scr. Mater.* 63, 488 (2010). https://doi.org/10.1016/j.scriptamat.2010.05.010.
14. A. Gueydan, B. Domengès, and E. Hug, *Intermetallics* 50, 34 (2014). https://doi.org/10.1016/j.intermet.2014.02.007.
15. J. Li, L. Liu, L. Deng, B. Ma, F. Wang, L. Han, and I.E.E.E. Electr, *Device Lett.* 32, 1433 (2011). https://doi.org/10.1109/LED.2011.2161749.
16. D. Zuo, S. Hu, J. Shen, and Z. Xue, *Mater. Des.* 58, 357 (2014). https://doi.org/10.1016/j.matdes.2014.02.004.
17. J. Zhang, B.-H. Wang, G.-H. Chen, R.-M. Wang, C.-H. Miao, Z.-X. Zheng, and W.-M. Tang, *Trans. Nonferr. Metal. Soc. China* 26, 3283 (2016). https://doi.org/10.1016/S1003-6326(16)64462-X.
18. O. Mokhtari and H. Nishikawa, *Microelectr. Reliab.* 113, 113942 (2020). https://doi.org/10.1016/j.microrel.2020.113942.
19. J.L. Murray, *Int. Metal. Rev.* 30, 211 (1985). https://doi.org/10.1179/imtr.1985.30.1.211.
20. R. Pretorius, A.M. Vredenberg, F.W. Saris, and R. de Reus, *J. Appl. Phys.* 70, 3636 (1991). https://doi.org/10.1063/1.349211.
21. R. Pretoriuos, C. Theron, A. Vantomme, and J.W. Mayer, *Crit. Rev. Solid State Mater. Sci.* 24, 1 (1999). https://doi.org/10.1080/10408439991329161.
22. E.T. Moiseenko, R.R. Altunin, and S.M. Zharkov, *Metall. Mater. Trans. A* 51, 1428 (2020). https://doi.org/10.1007/s11661-019-05602-5.
23. D.L. Zhang and D.Y. Ying, *Mater. Sci. Eng., A* 301, 90 (2001). https://doi.org/10.1016/S0921-5093(00)01388-5.
24. H.G. Jiang, J.Y. Dai, H.Y. Tong, B.Z. Ding, Q.H. Song, and Z.Q. Hu, *J. Appl. Phys.* 74, 6165 (1993). https://doi.org/10.1063/1.355183.
25. H.T.G. Hentzell and K.N. Tu, *J. Appl. Phys.* 54, 6929 (1983). https://doi.org/10.1063/1.332000.
26. H.T.G. Hentzell, R.D. Thompson, and K.N. Tu, *Mater. Lett.* 2, 81 (1983). https://doi.org/10.1016/0167-577X(83)90041-1.
27. Y. Guo, G. Liu, H. Jin, Z. Shi, and G. Qiao, *J. Mater. Sci.* 46, 2467 (2011). https://doi.org/10.1007/s10853-010-5093-0.
28. F. Haidara, M.-C. Record, B. Duployer, and D. Mangelinck, *Surf. Coat. Technol.* 206, 3851 (2012). https://doi.org/10.1016/j.surfcoat.2012.01.065.
29. D.P. Adams, M.A. Rodriguez, C.P. Tigges, and P.G. Kotula, *J. Mater. Res.* 21, 3168 (2006). https://doi.org/10.1557/JMR.2006.0387.
30. R.R. Altunin, E.T. Moiseenko, and S.M. Zharkov, *Phys. Solid State* 62, 621 (2020). https://doi.org/10.1134/S1063783420040034.
31. R.R. Altunin, E.T. Moiseenko, and S.M. Zharkov, *Phys. Solid State* 60, 1413 (2018). https://doi.org/10.1134/S106378341807003X.
32. R.R. Altunin, E.T. Moiseenko, and S.M. Zharkov, *Phys. Solid State* 62, 200 (2020). https://doi.org/10.1134/S1063783420010059.
33. S.M. Zharkov, E.T. Moiseenko, and R.R. Altunin, *J. Solid State Chem.* 269, 36 (2019). https://doi.org/10.1016/j.jssc.2018.09.009.
34. S.M. Zharkov, E.T. Moiseenko, R.R. Altunin, N.S. Nikolaeva, V.S. Zhigalov, and V.G. Myagkov, *JETP Lett.* 99, 405 (2014). https://doi.org/10.1134/S0021364014070145.
35. E.T. Moiseenko, R.R. Altunin, and S.M. Zharkov, *Phys. Solid State* 59, 1233 (2017). https://doi.org/10.1134/S1063783417060154.
36. S.M. Zharkov, R.R. Altunin, E.T. Moiseenko, G.M. Zeer, S.N. Varnakov, and S.G. Ovchinnikov, *Solid State Phenom.* 215, 144 (2014). https://doi.org/10.4028/www.scientific.net/SSP.215.144.
37. V.G. Myagkov, L.E. Bykova, O.A. Bayukov, V.S. Zhigalov, I.A. Tambasov, S.M. Zharkov, A.A. Matsynin, and G.N. Bondarenko, *J. Alloys Compd.* 636, 223 (2015). https://doi.org/10.1016/j.jallcom.2015.02.012.
38. V.G. Myagkov, V.S. Zhigalov, L.E. Bykova, S.M. Zharkov, A.A. Matsynin, M.N. Volochaev, I.A. Tambasov, and G.N. Bondarenko, *J. Alloys Compd.* 665, 197 (2016). https://doi.org/10.1016/j.jallcom.2015.12.257.
39. L.E. Bykova, S.M. Zharkov, V.G. Myagkov, V.S. Zhigalov, and G.S. Patrin, *JOM* 72, 2139 (2020). https://doi.org/10.1007/s11837-019-03919-5.
40. Powder Diffraction File (PDF 4 + , 2020), *Inorganic Phases Database, International Center for Diffraction Data (ICDD)* (Swarthmore, PA, USA). https://www.icdd.com/pdf-4/.
41. N. Kuwano, T. Doi, and T. Eguchi, *Trans. Jpn. Inst. Met.* 18, 807 (1977). https://doi.org/10.2320/matertrans1960.18.807.
42. C.D. Yang, W. Li, and W. Zhi, *Solid State Commun.* 151, 1270 (2011). https://doi.org/10.1016/j.ssc.2011.05.040.
43. F. Hodaj and A.M. Gusak, *Acta Mater.* 52, 4305 (2004). https://doi.org/10.1016/j.actamat.2004.05.047.
44. H. Xu, C. Liu, V.V. Silberschmidt, S.S. Pramana, T.J. White, Z. Chen, and V.L. Acoff, *Acta Mater.* 59, 5661 (2011). https://doi.org/10.1016/j.actamat.2011.05.041.

Publisher's Note Springer Nature remains neutral with regard to jurisdictional claims in published maps and institutional affiliations.